measured profiles of velocity components U and V, the turbulent kinetic energy k, and the dissipation rate of the turbulent energy ε, which is deduced from the equilibrium relation $\varepsilon = (0.3k)^{1.5}/l$. The values of the mixing length l are calculated from the data using its definition in terms of the mean-velocity gradient and the shear stress. The boundary conditions are that U at the wake edges is equal to the measured edge velocity U_e measured in the experiment, k and ε satisfy the zero-gradient conditions, $U_e\, dk/dx = -\varepsilon$ and $U_e\, d\varepsilon/dx = C_{\varepsilon 2}\varepsilon^2/k$, where $C_{\varepsilon 2}$ is one of the model constants. The configuration of the flow for which the calculation is made is depicted in Fig. 1. The wake-generating model is a flexible plate whose shape is varied to produce different pressure gradients on the upper and lower sides of the plate controlling the properties of the initial wake. The characteristics of the test flow at the trailing edge including the boundary layer thickness, the friction coefficient C_f, and the momentum thickness Reynolds number Re_θ are shown in Table 1. The details of the experiments and the results are given in Nakayama and Kreplin.[2] The step size in the calculation is initially taken about 0.5×10^{-3} times the momentum thickness θ_t at the trailing edge and is doubled at every 50th step until the step size of $0.2\theta_t$ is reached. About 1000 integration steps are needed to cover a distance of about $40\theta_t$ from the trailing edge, which is considered a near wake region.[3]

Results

The results of the calculation have been compared with the experimental data. Comparison of the developments of the mean velocity U, the turbulent kinetic energy k, and the turbulent shear stress $-\overline{uv}$ for the symmetric case, asymmetric case A, and asymmetric case C are shown in Figs. 2a, 2b, and 2c, respectively. The streamwise distance x is normalized by θ_t. In the symmetric wake case, the calculation results agree well with the experiment except for a minor underprediction of k and shear stress peaks. In the asymmetric case A, the mean velocity and k are predicted fairly well, although the shear stress on the thicker side are consistently underpredicted. In the strongly asymmetric case C, however, it is seen that the mean velocity profile is grossly underpredicted. The energy k is overpredicted on the thicker side and grossly underpredicted on the thinner side. It is seen that this is due to the slow growth rate calculated on the thinner side and faster spreading rate on the thicker side. Patel and Scheuerer[4] made similar a calculation for symmetric wakes and asymmetric wake generated by roughness on one side of a plate model and found relatively good agreement in the near wake region but prediction deteriorated downstream. They indicated that one reason for the poor performance of the k-ε model in wakes is due to its lack of representing the effects of the intermittency. Cho and Chung[5] incorporated the intermittency effects by their k-ε-γ model but a major improvement was not found. The present calculation indicates that even in near wakes, the prediction is poor when the asymmetry is severe. The data indicate that the size of turbulence on the thicker side is so large that the large eddies from this side also influence the spreading rate of the thinner side. The k-ε model which estimates the scale from the local values only cannot reflect the nonlocal effects of the large eddies. In test case C, these nonlocal effects are so strong that there is a transport of momentum and Reynolds stress in the direction opposite of the gradient.[2] The k-ε model fails to capture this phenomenon and is a reason for the poor performance in such highly asymmetric flows. The full paper contains evidence for this as well.

References

[1]Launder, B.E., and Spalding, D.B., "The Numerical Computation of Turbulent Flows," *Computer Methods in Applied Mechanics and Engineering*, Vol. 3, 1974, pp. 269–289.

[2]Nakayama, A., and Kreplin, H.-P., "Characteristics of Asymmetric Turbulent Near Wakes," *Physics of Fluids* (to be published).

[3]Ramaprian, B.R., Patel, V.C., and Sastry, M.S., "The Symmetric Turbulent Wake of a Flat Plate," *AIAA Journal*, Vol. 20, No. 8, 1982, pp. 1228–1235.

[4]Patel, V.C., and Scheuerer, G., "Calculation of Two-Dimensional Near and Far Wakes," *AIAA Journal*, Vol. 20, No. 7, 1982, pp. 900–907.

[5]Cho, J.R., and Clung, M.K., "A k-ε-γ Equation Turbulence Model," *Journal of Fluid Mechanics*, Vol. 237, 1992, pp. 301–322.

Time-Accurate Local Time Stepping Method Based on Flux Updating

X. D. Zhang,* J.-Y. Trépanier,† M. Reggio,‡ and R. Camarero§
École Polytechnique de Montréal, Montréal, Québec H3C 3A7, Canada

I. Introduction

TRADITIONALLY, a globally determined time step has been used in the prediction of unsteady compressible flows via explicit time-marching methods. The time increment established in this way, which is the smallest anywhere in the whole domain that satisfies the stability criteria, implies that for most of the cells only a fraction of their locally allowable time step is used to integrate the solution in time. Obviously, this is a waste of computational effort that should be avoided, especially when the ratio of local time steps spans many orders of magnitude, such as it does in problems requiring a highly variable node spacing and/or involving various scales of temperature. Moreover, the problem is in a deeper layer still: accuracy. For example, for a linear scalar equation solved with a first-order upwind scheme, a Courant-Friedrichs-Lewy (CFL) number equal to one leads to an exact representation of the original equation as higher-order error terms disappear, whereas in fact smaller CFL numbers result in a more diffusive solution.[1]

These simple facts tell us that to improve time-marching schemes for unsteady flow computations with regard to both computational effort and solution accuracy, a variable grid and physics-dependent time step size should be used that is as close as possible to the maximum time step dictated by the local CFL condition. Osher and Sanders[2] were among the first to propose a local time step (LTS) technique using a multistep predictor-corrector method. Their method is based on a grid refinement in time. For a grid that is refined by an integer of r in time, the scheme requires the storage of r-intermediate values, since an r-step predictor-corrector method is used to determine interface values. To overcome this drawback, Berger[3] has introduced interface equations to determine the interface values and to maintain the global conservation. With these methods, the assigned local time step distribution is fixed until the largest time step has been reached without consideration of any possible changes within this time period. This method of handling the problem may not be able to capture some rapidly incoming information at the proper time. In the work of Pervaiz and Baron[4] on reacting flow computations, an LTS approach that does not require a temporal interface equation has been described in which the rapidly incoming information is considered by simply restricting the cell time step to at most four times the minimum time step of the surrounding cells. More recently, Kleb et al.[5] generalized Berger's technique to two-dimensional Euler and Navier-Stokes equations for unstructured grids. To avoid complicated interface equations, Kleb et al.[5] have assigned a distribution of the local time steps that are integers with power-of-two multiples of the global minimum time step, such that for any adjacent time levels the grid is refined by two in time.

Although most of the LTS procedures have been shown to result in significant savings in computer time, little has been written about the major improvement in accuracy that can be obtained via

Received Aug. 11, 1993; revision received Feb. 24, 1994; accepted for publication Feb. 28, 1994.

*Research Associate, Department of Mechanical Engineering, C.P. 6079, Succ. A.

†Assistant Professor, Department of Mechanical Engineering, C.P. 6079, Succ. A. Member AIAA.

‡Associate Professor, Department of Mechanical Engineering, C.P. 6079, Succ. A.

§Professor, Department of Mechanical Engineering, C.P. 6079, Succ. A.

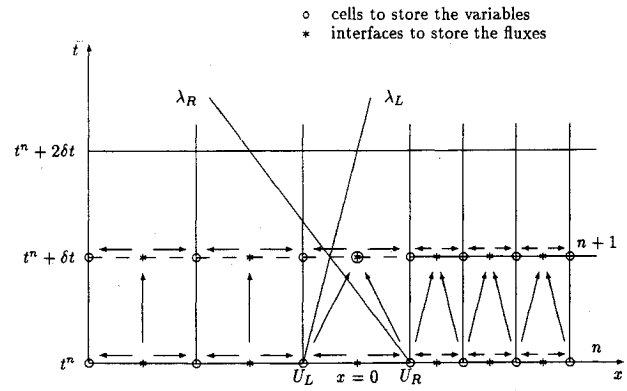

Fig. 1 Stencil for local time stepping.

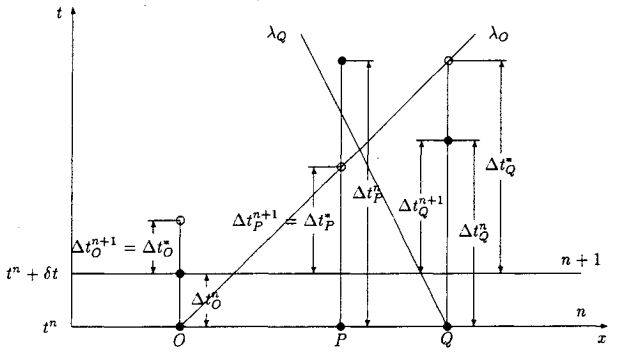

Fig. 2 Local time step re-evaluation.

the LTS method over the conventional global time step (GTS) method.

In this work, a new LTS approach based on a flux-updating procedure is presented. One of the main features of this approach is that, at each time level, the fluxes are updated according to the readjusted LTS distribution instead of a predetermined distribution. This feature provides a natural way of capturing the rapidly incoming information at the right moment and allows the use of local time steps very close to their maximum as given by local stability analysis. Thus it provides one with the ability to optimize the computational cost while simultaneously improving solution accuracy. The Euler solver used in this work is based on Roe's scheme[6] and is briefly recalled in Sec. II. The proposed LTS procedure is detailed in Sec. III. Computational tests for a one-dimensional shock tube and a two-dimensional blast wave using unstructured grids are presented in Sec. IV.

II. Numerical Scheme

The unsteady Euler equations can be written in the following matrix form:

$$\boldsymbol{U}_t + \nabla \cdot \mathcal{F} = 0 \tag{1}$$

in which $\boldsymbol{U}$ is the vector of conservative variables and $\mathcal{F}$ the flux matrix. Following a two-dimensional cell-centered finite volume discretization, the solution at cell P and at time level $(n + 1)$ is given by

$$\boldsymbol{U}_p^{n+1} = \boldsymbol{U}_p^n - \frac{\Delta t}{V_p} \sum_{k=1}^{N_{\text{sides}}} F_k^n L_k^n \tag{2}$$

where $\boldsymbol{F} = \mathcal{F} \cdot \boldsymbol{n}$ denotes the flux vector, $\boldsymbol{n}$ the unit outward normal vector, V_p the volume of cell P, and L_k the length of the kth side of V_p. The $\boldsymbol{F}_k$ flux vector on an interface is computed on the basis of left and right states according to the flux-difference splitting expression

$$\boldsymbol{F} = \frac{1}{2}(\boldsymbol{F}_R + \boldsymbol{F}_L) - \frac{1}{2}|\tilde{A}|(\boldsymbol{U}_R - \boldsymbol{U}_L) \tag{3}$$

where the computation of $|\tilde{A}|$ is carried out after Roe's[6] average. In this study, the right and left states have been considered to be piecewise constant, which leads to a first-order scheme.

III. Local Time Stepping

To simplify the following discussion, the one-dimensional Euler equations are used to outline the LTS flux updating procedure. For the ith cell, formula (2) becomes

$$\boldsymbol{U}_i^{n+1} = \boldsymbol{U}_i^n - \frac{\Delta t}{\Delta x_i}(\boldsymbol{F}_{i+1/2}^n - \boldsymbol{F}_{i-1/2}^n) \tag{4}$$

From a stability point of view, the time step increment Δt in Eq. (4) can be set to its local time step Δt_i instead of the smallest one, δt, throughout the domain. If we consider δt a step unit, then it can be seen that $k\delta t \le \Delta t_i < (k + 1)\delta t$ for some integer k. Therefore, the accurate local formula for calculating the intermediate values of U^{n+j} is

$$\begin{aligned} \boldsymbol{U}_i^{n+j} &= \boldsymbol{U}_i^n - \frac{j\delta t}{\Delta x_i}(\boldsymbol{F}_{i+1/2}^n - \boldsymbol{F}_{i-1/2}^n) \\ &= \boldsymbol{U}_i^n - \frac{\delta t}{\Delta x_i}\sum_{l=1}^{j-1}(\boldsymbol{F}_{i+1/2}^n - \boldsymbol{F}_{i-1/2}^n) \\ & \qquad j = 1, 2, \ldots, k \end{aligned} \tag{5}$$

As a counterpart, the conventional GTS method written for the $(n + j)$ time level reads

$$\begin{aligned} \boldsymbol{U}_i^{n+j} &= \boldsymbol{U}_i^{n+j-1} - \frac{\delta t}{\Delta x_i}(\boldsymbol{F}_{i+1/2}^{n+j-1} - \boldsymbol{F}_{i-1/2}^{n+j-1}) \\ &= \boldsymbol{U}_i^{n+j-1} - \frac{\delta t}{\Delta x_i}(\boldsymbol{F}_{i+1/2}^{n+j-1} - \boldsymbol{F}_{i-1/2}^{n+j-1}) \\ & \qquad j = 1, 2, \ldots, k \end{aligned} \tag{6}$$

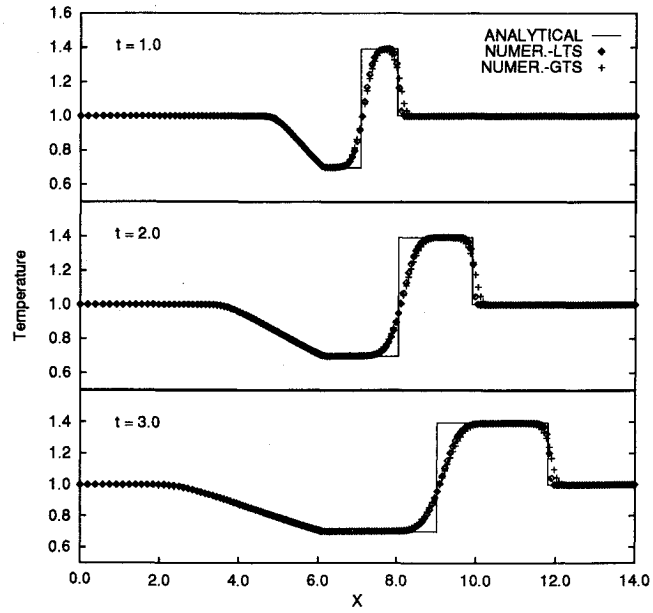

Fig. 3 Transient temperature distributions for one-dimensional shock tube, 220 points.

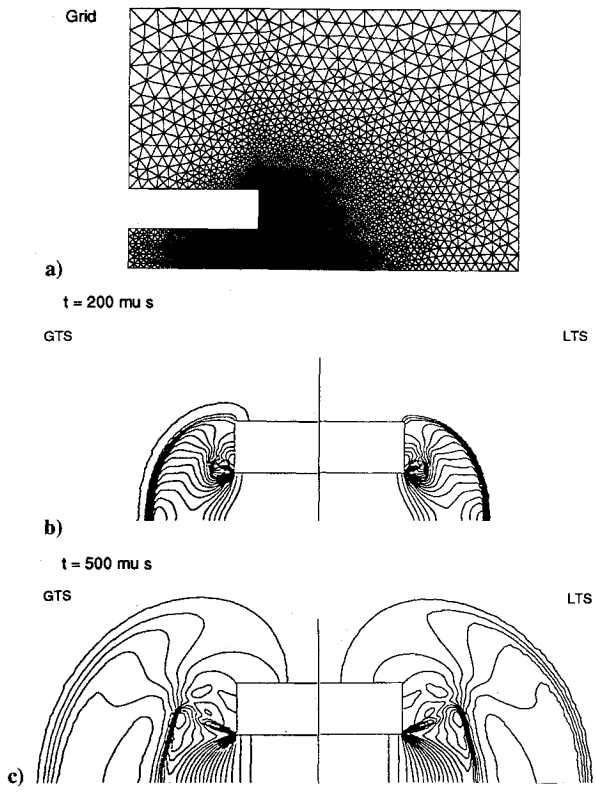

Fig. 4 Grid and temperature isolines for blast wave from a shock tube.

Note that if and only if $j = 1$, Eqs. (5) and (6) coincide. In fact, for advancing from time level n to time level $n + j$, the fluxes in Eq. (5) stay frozen at time level n, whereas in Eq. (6) these fluxes are updated and intermediate values at $(n + l)$ $(l = 1, 2, \ldots, j-1)$ are used. Since the flux calculation is generally the most expensive part of the computation, the benefit of using Eq. (5) instead of Eq. (6) can be clearly appreciated. Furthermore, extra flux calculations (corresponding to the use of small CFL number) may increase the truncation errors.[1]

Based on the preceding analysis, the proposed new LTS procedure is illustrated in Fig. 1 using a typical temporal stencil. In this figure, the circles indicate the location of the conservative variables whereas the stars denote the interfaces where the fluxes are stored. Let us start the discussion from time level n. From the solution at time level $(n - 1)$, the fluxes can be computed and stored at all of the starred locations. Then $\boldsymbol{U}^n$ is evaluated from Eq. (4) and stored on all cells at time level n. From local stability analysis, the maximum allowable local time step Δt_i is assigned to each cell. After choosing the minimum, $\delta t = \text{Min}\,(\Delta t_i)$, as the global time increment, the cells are divided into two groups according to

$$G_1 = \{i | \Delta t_i \leq 2\delta t\}, \qquad G_2 = \{i | \Delta t_i > 2\delta t\}$$

In Fig. 2, G_1 includes the cells with $x > 0$, and the rest belong to G_2.

For the next time level, the fluxes at the interfaces within G_1 must be updated from Eq. (3) using the data on the n level. In G_2, the fluxes can be taken directly from the previous step instead of applying Eq. (3) because they are outside the affected regions. Only the interface between the two regions requires particular attention, but there is no further difficulty if it is included in G_1. Thus, this flux should be computed using Eq. (3). This completes the evaluation of the fluxes, and the variables $\boldsymbol{U}^{n+1}$ can then be calculated directly from Eq. (2).

To proceed to the next time level, the local time step distribution needs to be re-evaluated such that quickly propagated information can be captured at the proper moment. It should be pointed out that this re-evaluation is necessary, as illustrated in Fig. 2. At time level $t = t^n$, cells O, P, and Q have different local time steps, Δt_O^n, Δt_P^n, and Δt_Q^n, respectively. A small Δt_O^n relative to Δt_P^n indicates that at least one of the propagating wave speeds at cell O is much greater than that at cell P. This implies that the information at cell O may be propagated to cell P before $t_n + \Delta t_P^n$ has been reached. Therefore, the local time step at cell P must be modified at that moment to account for the incoming information. This modification is made by readjusting the local time steps Δt^* after each time step. Without loss of generality, suppose that the information at cell O reaches cell P at the next time level $t = t^{n+1}$, then the proper local time step Δt_P^{n+1} is re-evaluated as $\Delta t_P^{n+1} = \text{Min}\,\{(\Delta t_P^n - \delta t), \Delta t_P^*\}$.

After the new local time step distribution $\{\Delta t^{n+1}\}$ has been evaluated, the previously stated procedure is repeated until the maximum time step has been reached and this completes a global time-marching cycle. Following this, the fluxes at every interface are updated using Eq. (3). Within each global cycle, the time marching can be regarded as local cycles since only part of the fluxes need to be updated. Generalization of this procedure to two-dimensional unstructured grids is straightforward.

IV. Numerical Tests

A. One-Dimensional Shock-Tube Problem

The first test case is a one-dimensional shock-tube problem. The computation was conducted at a density and pressure ratio of 10. The initial jump was positioned at $x = 6.1$ within the computational domain of [0,14]. To show the efficiency of the LTS method, nonuniform grid spacing was used to increase the ratio of the LTS. Ninety-five points were located within [0, 6.1] with a stretching factor of $\alpha = 0.97$, i.e., $\Delta x^{i+1} = \alpha \Delta x^i$, and 125 points were placed uniformly within [6.1,14].

The transient behavior of the temperature distribution at $t = 1$, $t = 2$, and $t = 3$ is shown in Fig. 3. The CPU time ratio of the GTS over the LTS method used to compute the fluxes until $t = 3$ is about 2.74. The accuracy improvement is evident, as revealed by the results depicted in these figures. It seems that the accuracy improvement of the LTS solutions is more significant near the shock, where much fewer points are involved across the shock as compared to GTS solutions.

B. Two-Dimensional Blast Wave from a Shock Tube

The second problem involves an axisymmetric blast wave which exits from a cylindrical shock tube. This configuration is well documented in Ref. 7. The purpose of this computation is to show the capability and efficiency of the LTS method for unsteady two-dimensional problems with unstructured grids. The computational grid, which is shown in Fig. 4, has a total of 9657 triangles with a higher concentration near the tube exit.

A shock wave was initially positioned inside the tube and the time when the shock wave exits the tube is referenced to zero. Temperature isolines are also presented in Fig. 4 for $t = 200$ μs and $t = 500$ μs, respectively. Once again it can be seen that the LTS approach has appreciably improved solution accuracy as indicated by a sharper shock in comparison with the result obtained using the GTS procedure. Moreover, the computational speed of this LTS method is about 2.2 times faster than that of the GTS method.

References

[1]Hoffmann, K. A., *Computational Fluid Dynamics for Engineers*, Engineering Education System, Austin, TX, 1989, pp. 166–214.

[2]Osher, S., and Sanders, R., "Numerical Approximations to Nonlinear Conservation Laws with Locally Varying Time and Space Grids," *Mathematics of Computation*, Vol. 41, No. 164, 1983, pp. 321–336.

[3]Berger, M. J., "On Conservation at Grid Interfaces," *SIAM Journal on Numerical Analysis*, Vol. 24, No. 5, 1987, pp. 967–984.

[4]Pervaiz, M. M., and Baron, J. R., "Spatio-Temporal Adaption Algorithm for Two-Dimensional Reacting Flows," *AIAA Journal*, Vol. 27, No. 10, 1989, pp. 1368–1376.

[5]Kleb, W. L., Batina, J. T., and Williams, M. H., "Temporal Adaptive Euler/Navier-Stokes Algorithm Involving Unstructured Dynamic Meshes," *AIAA Journal*, Vol. 30, No. 8, 1992, pp. 1980–1985.

[6]Roe, P. L., "Approximate Riemann Solvers, Parameter Vectors, and Difference Schemes," *Journal of Computational Physics*, Vol. 43, No. 2, 1981, pp. 357–372.

[7]Cooke, C. H., and Fansler, K. S., "Comparison with Experiment for TVD Calculations of Blast Waves from a Shock Tube," *International Journal for Numerical Methods in Fluids*, Vol. 9, No. 1, 1989, pp. 9–22.

Turbulent Flow Measurements with a Triple-Split Hot-Film Probe

M. D. Doiron* and D. W. Zingg†
University of Toronto, Toronto, Ontario M3H 5T6, Canada

Nomenclature

A_{jk}	= asymmetry correction factor
$a_0,\ldots,a_3$	= polynomial coefficients for velocity magnitude
$b_{i,0},\ldots,b_{i,6}$	= Fourier series coefficients for velocity direction, $i = 1, 2, 3$
$c_{i,j,0},\ldots,c_{i,j,3}$	= polynomial coefficients for velocity direction Fourier series coefficients, $i = 1, 2, 3$ and $j = 0, 1,\ldots,6$
$d_0,\ldots,d_{10}$	= Fourier series coefficients for correction factor
E_i	= output voltage for individual sensor, $i = 1, 2, 3$
$e_{k,0},\ldots,e_{k,2}$	= polynomial coefficient for correction factor Fourier series coefficients, $k = 0, 1,\ldots,10$
U	= velocity magnitude
α	= angle of attack
ΣE_i^2	= sum of the squares of the sensor voltages
Θ	= azimuthal or flow angle

Introduction

COMPLEX turbulent shear flows occur in many aerospace applications, such as aerodynamic devices and gas turbine engines. Measurements of mean and fluctuating velocity components can greatly aid our understanding of such flows. Experimental data are particularly useful in assessing and validating turbulence models used in computational fluid dynamics codes. Velocity measurements are generally made using a pitot-static tube, a constant temperature hot-wire anemometer, or a laser Doppler anemometer (LDA). For separated turbulent flows, pitot-static tubes and conventional hot-wire probes are generally inapplicable.[1] Because of the high cost of LDA measurements, modified hot-wire techniques have been developed which are suitable for reversed flows. These include pulsed hot wires[2] and flying hot wires.[3] Disadvantages of these approaches are discussed by Nakayama.[4]

Triple-split hot-film probes are a potentially useful alternative for velocity measurements in separated turbulent flows. Such probes typically consist of three separate films deposited on a cylinder. The operating principle is based on the variation of the local heat transfer coefficient on a cylinder with the magnitude and direction of the oncoming flow velocity. Most studies involving split-film anemometry have been with double-split hot-film probes. These operate on the same principle but retain the directional ambiguity of conventional hot wires and, hence, are not applicable to separated turbulent flows. The results of these studies indicate that split-film probes provide comparable accuracy to hot-wire probes for mean velocities but have a more limited frequency response.[4] Despite their potential, especially for measurements of mean velocities, triple-split hot-film probes have received little use. The only example of their use known to the authors is reported by Modera,[5] who used a triple-split probe for low-frequency reversed flow measurements over a 0–8 m/s flow speed range. The purpose of this Note is to demonstrate that the triple-split hot-film probe can be very useful for measurements of mean velocities in separated turbulent flows. Further details of the present study are given in Ref. 6.

Received June 28, 1993; revision received April 14, 1994; accepted for publication April 19, 1994.

*Research Assistant, Institute for Aerospace Studies, 4925 Dufferin St.
†Assistant Professor, Institute for Aerospace Studies, 4925 Dufferin St. Member AIAA.

Calibration Procedure

The triple-split hot-film probe used (Dantec model 55R94) consists of three nickel films deposited on a 400-μm-diam quartz cylinder, with each film occupying approximately 120 deg of the circumference as shown in Fig. 1. As such, the probe can resolve two-dimensional velocity components in a plane perpendicular to the axis of the probe for any flow angle Θ through a full 360 deg. The calibration procedure is described in detail in Ref. 6. It is largely based on the method of Jørgensen,[7] with an extension to account for asymmetries in the characteristics of the probe. A calibration rig that is capable of providing a range of known flow speeds and flow angles, through 360 deg, is necessary for the calibration.

With a perfectly symmetric probe, the calibration scheme could allow for independent determination of the magnitude and direction of the velocity. However, actual probes can have asymmetries resulting from mismatched films, imbalances in film temperatures and sensitivities, and probe body effects. These effects generally couple the determination of the velocity magnitude and direction. Expressions will first be given that assume the independence of the magnitude and direction. A correction factor will then be incorporated that couples magnitude and direction determination through an iterative procedure. All curve fits were performed using the least squares method.

The calibration is carried out at a number of flow speeds, typically 6, spanning the range of foreseeable test speeds. For each given calibration speed, the calibration is performed at a number of flow angles, typically 18, evenly spaced through the full 360 deg. The sum of the squares of the sensor voltages ΣE_i^2 is a measure of the total heat convected from the probe and is ideally not influenced by flow direction. This initial assumption is important since the average value of ΣE_i^2 over all flow angles for a given flow speed was used for calibration purposes. The velocity magnitude is determined from the following third-order polynomial in ΣE_i^2,

$$U = a_0 + a_1(\Sigma E_i^2) + a_2(\Sigma E_i^2)^2 + a_3(\Sigma E_i^2)^3 \tag{1}$$

The velocity direction is determined by modeling the angular response of each of the three sensors by a third-order Fourier series, as follows.

$$E_i(U,\Theta) = b_{i,0} + b_{i,1}\cos\Theta + b_{i,2}\cos 2\Theta + b_{i,3}\cos 3\Theta + b_{i,4}\sin\Theta + b_{i,5}\sin 2\Theta + b_{i,6}\sin 3\Theta \tag{2}$$

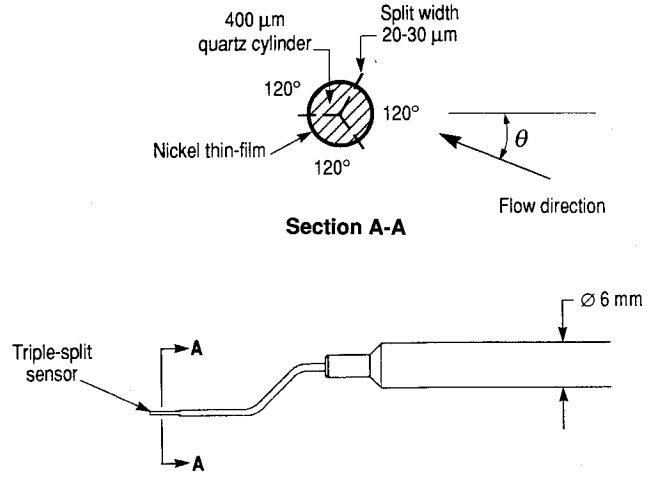

Fig. 1 Triple-split hot-film probe.